

Tan, Aditya Suryadi; Rabel, Fabian; Sattel, Thomas; Sill, Yannick Lee;  
Goldasz, Janusz

**Design and performance investigation of a novel 3DOF compact MR damper**

---


*Original published in:* Smart materials and structures. - Bristol : IOP Publ.. - 31 (2022), 12, art. 125020, 14 pp.  
*Original published:* 2022-11-21  
*ISSN:* 1361-665X  
*DOI:* [10.1088/1361-665X/aca12f](https://doi.org/10.1088/1361-665X/aca12f)  
*[Visited:* 2023-05-09]



This work is licensed under a [Creative Commons Attribution 4.0 International license](https://creativecommons.org/licenses/by/4.0/). To view a copy of this license, visit <https://creativecommons.org/licenses/by/4.0/>

---

# Design and performance investigation of a novel 3DOF compact MR damper

Aditya Suryadi Tan<sup>1,\*</sup> , Fabian Rabel<sup>1</sup>, Thomas Sattel<sup>1</sup>, Yannick Lee Sill<sup>1</sup> and Janusz Goldasz<sup>2</sup>

<sup>1</sup> Mechatronics Group, Department of Mechanical Engineering, Technische Universität Ilmenau, Max-Planck-Ring 12, Ilmenau, 98693, Germany

<sup>2</sup> Cracow University of Technology, Warszawska 24, 31-155 Cracow, Poland

E-mail: [aditya-suryadi.tan@tu-ilmenau.de](mailto:aditya-suryadi.tan@tu-ilmenau.de)

Received 13 July 2022, revised 18 October 2022

Accepted for publication 7 November 2022

Published 21 November 2022



CrossMark

## Abstract

Magnetorheological (MR) fluid based dampers have been established as an alternative to classical hydraulic dampers with proportional electromagnetic valves under vibration processes which demand adaptive damping forces. Almost all MR-dampers are spatially 1-degree-of-freedom (DOF) dampers, having only one axis or direction of damping force generation. In many technical applications there exist movements in more than one spatial DOF, eventually necessitating more than one damper. Because of this, the damping is required not only in one but in more spatial directions, yet adjustable. In this work, a new design of a spatial 3DOF MR damper is proposed to allow damping in three directions within one damping device. The underlying motivation is to spatially integrate three damping directions in one device to potentially reduce installation space compared to three separate 1DOF dampers. The basic idea of the construction is to use one fluid chamber with several spatially distributed control elements at different positions of the fluid chamber. The control elements are electromagnets, generating the magnetic field in the fluid at different positions so that in total three spatial DOFs can be damped individually. Experiments and investigation are made, where the damper's behavior are analyzed not only in one single DOF but also in more than one DOF. It is shown, that the damping concept can generate damping in all three spatial DOFs, both individually or together. Moreover, the damping can be generated to be dominant in one specific direction, meanwhile minimum in the other direction orthogonal to it.

Keywords: magnetorheological fluid, three degrees-of-freedom, 3DOF, adjustable damping, compact design, prototype

(Some figures may appear in colour only in the online journal)

## 1. Introduction

Magnetorheological (MR) fluid-based dampers have been proven as an excellent damping technology due to their ability

\* Author to whom any correspondence should be addressed.



Original Content from this work may be used under the terms of the [Creative Commons Attribution 4.0 licence](https://creativecommons.org/licenses/by/4.0/). Any further distribution of this work must maintain attribution to the author(s) and the title of the work, journal citation and DOI.

to adapt the generated damping force based on different application requirements [1, 2]. By adjusting the generated damping, the vibration that occurs along its damping axis can be reduced or even avoided in an optimal way. Up to this point, more and more MR-based dampers with various structure designs [3] including mathematical models [4] have been investigated. However, most of the damper design results in a 1-degree-of-freedom (DOF) MR damper, whereby the generation of the damping is possible only in one direction.

In many technical applications, such as in the automotive industry, civil engineering, military, railway, or even medical

technology, there exists a movement in more than one spatial DOF. In some cases, the movement and therefore the vibration could happen even in all of the six existing spatial DOFs. An example is the body of a vehicle due to a bad road condition [5], a bridge due to turbulence caused by wind [6], or even a washing machine due to the unbalance rotating mass [7]. In these mentioned cases, the vibration occurs in more than one direction. Because of this reason, damping is required not only in one direction but also in all of the movement possible directions, yet adjustable.

In the most common way, several one-directional MR dampers will be implemented, at least one in each operating DOF's axis [8, 9]. By doing so, the damping can be provided and controlled in each spatial DOF axis. Another way is to integrate several one-directional MR damper elements in one damper system so that the one damper system can operate in several spatial DOFs [10]. Normally, such a damper system is applied as haptic systems, where dissipation in a form of feedback force for the user is required in more than one direction. The number of DOFs varies from 2DOF [11], 3DOF [12, 13], or even 4DOF [14, 15], depending on the requirements. However, using this method, the higher the number of the DOF of the damper system, the bigger the total device volume of the damper system.

In this work, a new MR damper design with three-spatial-DOFs integrated into one device is proposed. The basic idea of the construction is to arrange several control elements at different locations of one fluid chamber. The control element is an electromagnet and each element generates a magnetic field for the MR damper. By such an arrangement the magnetic field and therefore the damping effect can be generated in more than one DOF's axes, both individually and together. A possible benefit of such a damper concept could be a compact design compared to three single-DOF dampers. Due to the underlying working principle, the proposed damper concept possesses a possibility to be scaled up or down, based on the stroke requirements. This can be done by simply changing the length of the connector rod.

An overview of the damper structure and configuration will be discussed in section 2. A derivation of a known operating mode that is used as a benchmark for this work will be elaborated in the third section. The experimental setup for this work including each measurement procedure together with its respective experimental results will be presented and discussed in the fourth section. Additionally to that, a comparison to the known operating mode will also be shown. In the fifth section, the whole work will be summarized and concluded and an outlook for future works will be given.

## 2. Proposed 3DOF MR damper

In this section, the construction of the proposed damper itself, the damper medium, and the components used in the experiment are elaborated.

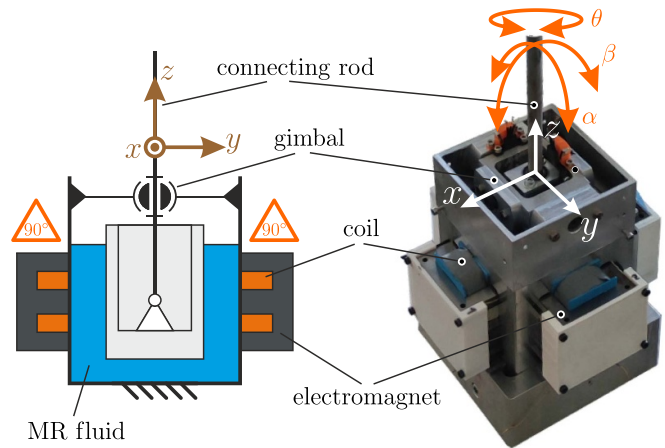


**Figure 1.** Principle sketch (left) and photo (right) of the constructed compact 3DOF MR damper.

### 2.1. Construction of the MR damper

Figure 1 depicts the principle sketch and the constructed proposed 3DOF MR damper. The spatial rotational DOFs are shown in this figure by the orange arrows ( $\alpha, \beta, \theta$ ).

A spatially fixed  $xyz$ -Cartesian coordinate system is added in the figure to show the orientations for axes of rotation and directions. As it can be seen in this figure, the damper has a shape of a box. At the damper's wall, four electromagnets are installed on the four sides of the damper, one electromagnet on each side, except the top and the bottom side. The bottom side is used as the mount of the damper and the top side is used as an access for the damper to be connected with a moving system. Each electromagnet is driven by an independent power supply so that the electromagnets can be activated and therefore the magnetic field can be applied individually on the four sides of the box. By using this configuration, the magnetic field can be generated either on all four sides or only on one desired side of the damper. In figure 1(left) the electromagnets view does not represent their arrangement in the experimental setup in figure 1(right). The correct representation of the electromagnet arrangement is depicted in figure 2(left). However, the view of the electromagnets and the magnetic field in figure 1(left) are rotated by  $90^\circ$  for a better view of the magnetic field lines. This is indicated by the orange triangle symbol. This rotated view is also conducted for subsequent figures (see figures 11, 15, and 17).

The housing box itself is none other than the fluid chamber, where the MR fluid is contained. Figure 2 shows the cross-section of the box in the  $xy$ -plane. The fluid chamber has a dimension of  $78 \text{ mm} \times 78 \text{ mm} \times 100 \text{ mm}$ . In the middle of the fluid chamber, a *plunger* with a dimension of  $56 \text{ mm} \times 56 \text{ mm} \times 84.5 \text{ mm}$  is inserted. This means that each side of the plunger has an equal distance to the wall of  $11 \text{ mm}$  when the plunger is exactly in the middle of the fluid chamber. The plunger can be moved in any direction on the  $xy$ -plane, causing the MR fluid to be squeezed in different directions. The height of the

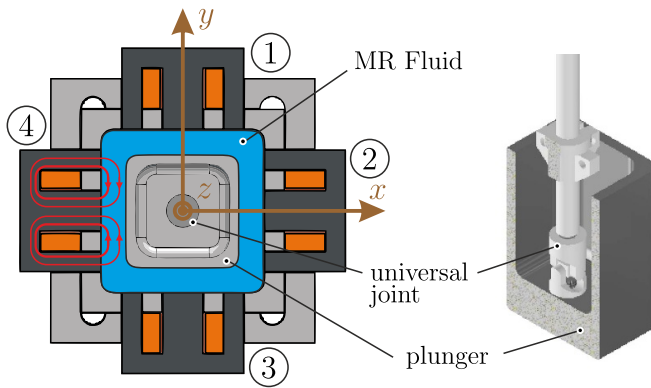


**Figure 2.** Cut section of the damper in  $xy$ -plane (left) and 3D-cut section (right) of the damper's plunger.

fluid chamber and the damper's plunger can be any length, as long as it is enough to contain the fluid in the chamber during its operation. The state of the squeezed MR fluid in a specific region can be altered by activating the respecting electromagnet, that is attached to each side of the fluid chamber. As an example, the left electromagnet, No. 4, in figure 2 is activated, generating a magnetic field only on the left side of the plunger. This solidifies the MR fluid locally in the region where there is magnetic field exists and therefore increases both the flow resistance of the MR fluid in this area and the movement resistance of the plunger in this direction. Additional to that, the plunger is 3D-printed and made of a non-magnetic material. This eliminates the attraction force from the magnet to the plunger. With this configuration, the generated force is a pure damping force from the squeezed MR fluid in the respective movement direction. In figure 2(right), there is another cross-section that shows that the plunger is connected to a rod via a universal joint. This joint is mounted at the center of the mass of the plunger. By doing so, the mass surface could be held to be as parallel as possible to the wall of the fluid chamber during its movement.

The geometry parameters of the proposed MR damper are listed again in table A1, giving a better overview of the overall dimensions of the damper.

## 2.2. Gimbal mechanism

The connecting rod is mounted to the damper via a *gimbal mount*, as shown in figure 1. The gimbal mount is used to decouple the combined movement of the rod in  $xy$ -plane so that the movement of the rod can be measured individually on each movement axis. The gimbal mechanism design is shown in figure 3, where all components responsible for the movement in the same direction are presented with an equal color. As it can be seen in the figure, there are three colors for the three-movement that are allowed through this mechanism. In this work, the orange, blue and green parts are the ones responsible for the movement about the  $x$ ,  $y$ , and  $z$ -axis respectively. The dark orange and the dark blue parts are the sensors to measure the angle  $\alpha$  and  $\beta$  for the angular movement about the  $x$ - and  $y$ -axis respectively. The sensor

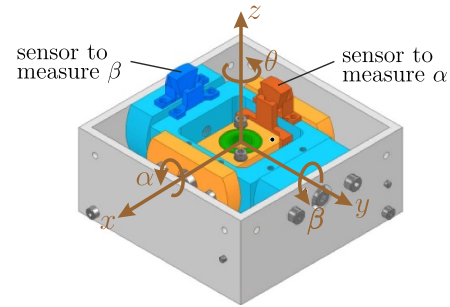


**Figure 3.** Design of the gimbal mechanism with colors, where each color corresponds to a particular degree-of-freedom.

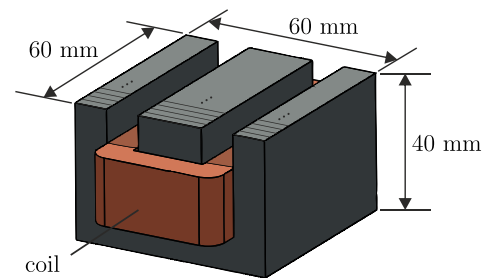


**Figure 4.** Sketch of the electromagnet showing the total dimension and its operating area.

is a Hall sensor SS495A1, which is installed between two Neodym block magnets. The rotation of the rod about the gimbal will change the position of the Hall sensor and therefore the strength of the magnetic field measured by it. Based on the read magnetic field, the angles  $\alpha$  and  $\beta$  can be determined. The angle  $\theta$  for the movement about the  $z$ -axis will be measured by an encoder separately. Since the connecting rod can be rotated in all three rotational axes ( $\alpha$ ,  $\beta$  and  $\theta$ ), the proposed MR damper is defined to have three DOFs.

## 2.3. Electromagnet and magnetic field analysis

The electromagnet used in this damper concept is an electromagnet, whose core is of the E-shape. The iron core consists of 120 sheets of EI60-lamination cores. Each sheet has a thickness of 0.5 mm. As it can be seen in figure 4, by using this configuration, the electromagnet has an operating area of 60 mm  $\times$  60 mm. To generate the magnetic field, a coil is inserted into the E-profile. The coil is a winding of a copper wire with a wire diameter  $d_{Cu}$  of 0.63 mm. The number of winding  $N_c$  for each electromagnet is 315 winding. Using this wire, the maximum current given to the coil is limited by the allowable current density  $J_{alw}$ , where

$$I_{max} = J_{alw} A_{Cu} = J_{alw} \frac{1}{4} \pi d_{Cu}^2. \quad (1)$$

With a chosen  $J_{alw} = 8 \text{ A mm}^{-2}$ , the maximum current is  $I_{max} = 2.5 \text{ A}$ . Based on this calculation and safety consideration, the experiments will be conducted with a maximum excitation current of  $I_{max} = 2.4 \text{ A}$ .

Since the damper's plunger is not made of a ferromagnetic material, the magnetic field will dominantly flow only through

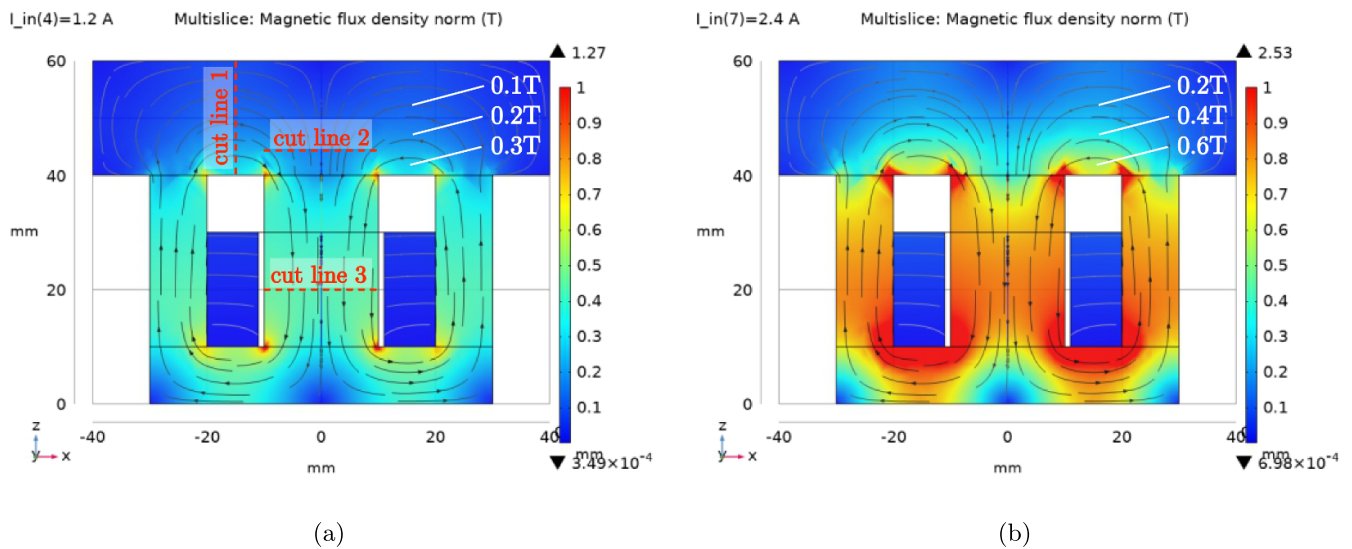


**Figure 5.** FEM-analysis results to determine the operating range of the electromagnet with an input current of (a) 1.2 A and (b) 2.4 A.

the MR fluid, as such there exists no pulling force acting on the plunger. Figure 5 shows the finite element method (FEM) analysis of the magnetic field using COMSOL Multiphysics 5.6. As it is presented in the figure, the magnetic field in the MR fluid will have a form of a bow, flowing between the outer and the inner pole of the E-iron core of the E-magnet. A block of an MR fluid used in this work with a dimension of  $20\text{ mm} \times 80\text{ mm} \times 80\text{ mm}$  is put on the electromagnet to estimate the operating range of the generated magnetic field. The property of the MR fluid is set to be the one used in this work. It can be seen in the results, that by using this electromagnet configuration, the magnetic field has approximately two-thirds of its maximum magnitude at a distance of about 10 mm from the surface of the iron core. Further than that, the magnetic field became much smaller. Using this consideration, the distance between the plunger and the damper's wall is chosen to be 11 mm in this work, with an assumption that a significant change in the force for increasing the magnetic field can still be seen in the measurement.

#### 2.4. Construction summary

In summary, based on the above explanations, the proposed MR damper possesses four control elements (the electromagnets) that are integrated into one fluid chamber yet are installed in four different locations of the damper. By using this design, the damper could operate in three DOFs, which are the three rotational directions ( $\alpha$ ,  $\beta$ , and  $\theta$ ). This means that the damping can be generated in three different directions by using one single damper element. Moreover, the integration of multiple control elements in one fluid chamber opens a possibility for the damper to have a more compact structure. The damping behavior of the proposed MR damper will be investigated via experiments. The advantages and disadvantages of the design will also be discussed based on the experimental results in the next sections.

**Table 1.** Physical properties of the magnetorheological fluid AMT-SMARTEC<sup>+</sup>.

Physical property	Value	Unit
Dynamic viscosity $\eta$	0.37	Pa·s
Relative permeability $\mu_r$	12	—
Density $\rho$	2.9	kg l <sup>-1</sup>
Operating temperature $T$	-20 to 150	°C
Yield stress $\tau_0$ at $B = 1.38\text{ T}$	69	kPa

### 3. MR fluid

The basics about MR fluids are summarized e.g. in [1]. In general, MR fluid is a suspension of magnetic particles in a carrier fluid. In the presence of a magnetic field, the particles will build a chain-like structure parallel to the magnetic field direction. This chain-like structure will increase the flow resistance of the fluid. The operating mode of the fluid is classified by how these particle chains are deformed. In this section, the properties of the utilized MR fluid are stated and the applied operating mode will be elaborated.

#### 3.1. MR fluid characteristic

The fluid that is used in this work is MR fluid AMT-SMARTEC<sup>+</sup> from Arus MR Tech [16], whose properties are enlisted in table 1. From the datasheet of the fluid, the relation between the applied magnetic field density  $B$  in Tesla and the generated MR fluid yield stress  $\tau_0$  in kPa

$$\tau_0 = -11.56B^3 + 16.15B^2 + 49.76B \quad (2)$$

can be found, where the yield stress of the fluid is a third-order polynomial function of the magnetic field density. The relative permeability is obtained from the  $B$ - $H$  relation of the MR fluid and assumed to be constant up to a magnetic flux density  $B = 0.8\text{ T}$ .

3.2. Mixed squeeze-pinch operating mode

In the previous section, it is mentioned that the MR fluid will be squeezed by the damper’s plunger. Therefore, from a fluid mechanics perspective, the operating mode for this damper is a squeeze mode. However, from a magnetostatics perspective, the magnetic field lines relative to the fluid flow direction are similar to a pinch mode operation [17, 18]. Figure 6 depicts the configuration comparison between the conventional squeeze mode, figure 6(a), and the squeeze mode used in this work figure 6(b). The conventional squeeze mode in figure 6(a) has a magnetic field applied perpendicularly to the flow direction of the fluid and the squeezing surface [3]. Therefore, the squeeze operating mode can be assumed as a flow operating mode in a rectangular channel with varying gap sizes and the channel’s width [19, p 246]. In this work, the direction of the applied magnetic field is not perpendicular to the flow direction. As it has been proven by the FEM analysis (see figure 5) and shown in figure 6(b), the magnetic field has a form of an arc. In giving a better visualization of this, the values of the magnetic flux density  $B$  in three different cut-lines with increasing applied current  $I$  are evaluated. The three cut-lines are plotted in figure 5(a). The line-average values of the magnetic flux density  $B$  for three different cut-lines are plotted in figure 7. The color represents the cut-lines, meanwhile, two different marks are used to represent the two different components of the flux density. The cross and circular marks are used to label the  $z$ - and the  $x$ -component of the magnetic flux density respectively. As it can be seen in this figure, for cut-line No. 1, the  $z$ -component of the flux density is zero, meanwhile the  $x$ -component increases as the current increase. It means that the magnetic field direction is parallel to the squeezing surface. For the cut-line No. 2, the opposite happens. The magnitude of the flux density for the  $z$ -component increases as the current is increased. The negative direction shows that the magnetic field is generated downwards. It means that the magnetic field direction is perpendicular to the squeezing surface. These two cut-lines verifies the arc-like structure of the magnetic field for the squeeze mode used in this work (see figure 6(b)). Cut-line No. 3 is there to show that for the applied current of 2.4 A, the iron core of the electromagnet has not been saturated.

The difference in the magnetic field lines orientation of both operation modes made the chain-like structure of the MR fluid to also have a different orientation. As it is depicted in the figures, the conventional one has a chain-like structure in the form of a pillar, whereas the other has a chain-like structure in the form of an arc. Therefore, the operation mode used in the proposed damper, figure 6(b), is a mixture between a squeeze mode and a pinch mode, and will be named a *mixed squeeze-pinch operation mode*.

Since the operating mode is different, the squeeze mode equation in the literature [3, 20, 21] cannot be directly implemented for this setup. Moreover, in comparison to the damper design of MR damper using the squeeze mode in general, the squeezing plate will have a circular surface [20, 21], in which the flow will be symmetrical in the radial direction. In this work, the squeezing surface has a quadratic form. Based on these reasons, building a mathematical model is considered to

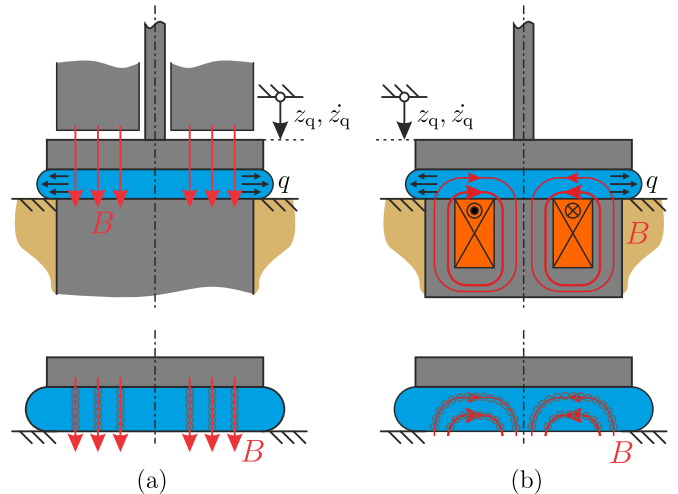


Figure 6. Configuration comparison between (a) the conventional squeeze mode and (b) the one used for the proposed damper in this work, the *mixed squeeze-pinch operation mode*. The coordinate  $z$  is a new one and does not correspond to those in the other figures.

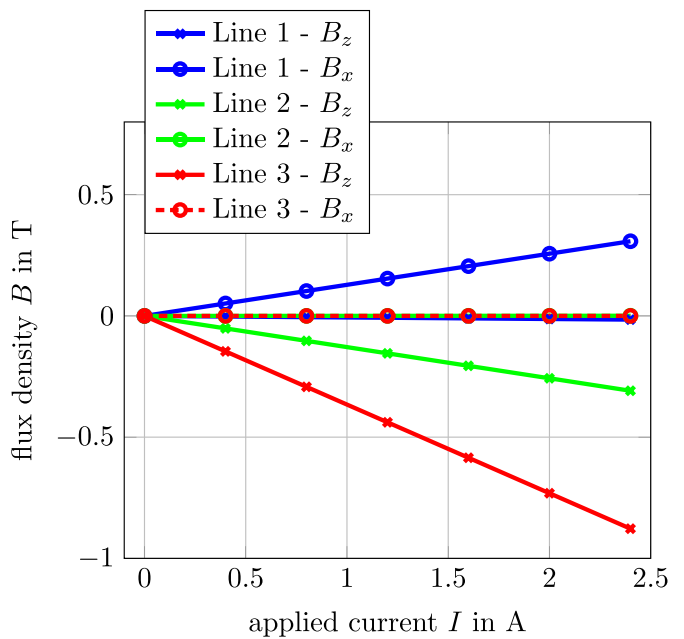
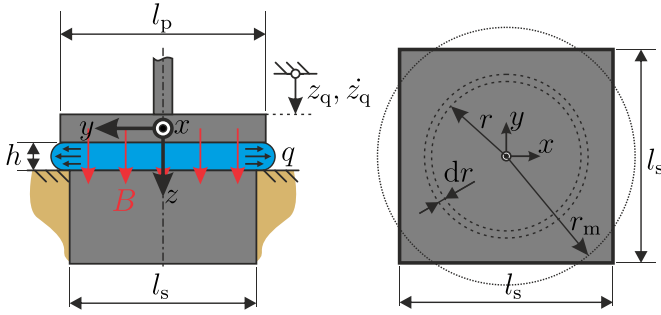


Figure 7. Simulation results of the average magnetic flux density for different cut-lines.

be difficult and the modeling of such a *mixed squeeze-pinch mode* is suggested to be solved numerically.

In this work, a derivation of the analytical mathematical model for the conventional squeeze mode in figure 6(a) is presented. This model will not be applied for the combined squeeze-pinch mode in figure 6(b) because of the aforementioned comment. The calculated damping force under conventional squeeze mode operation will be compared to the experimentally obtained damping force under mixed squeeze-pinch mode operation. By doing so, an insight into how big is this *mixed squeeze-pinch force* in comparison to the conventional one can be obtained. The conventional squeeze mode model is



**Figure 8.** Configuration of the squeeze mode using quadratic squeezing surface.

derived under the assumption that the applied magnetic field operates in the orthogonal direction of the squeezing surface and is homogeneous over the whole squeezing surface. Due to the difference in the surface shape between a conventional circular squeeze mode damper and the quadratic damper surface given here, corner effects of the quadratic surfaces are neglected, but an averaged circular surface is assumed to reduce the modeling error. Figure 8 shows the principle sketch of a conventional squeeze mode with a quadratic surface. The magnetic field is applied over the quadratic surface with a side length of  $l_s$ . The squeezing surfaces are separated by the gap  $h$ . It is assumed that the MR fluid flows from the middle point to the edges of the quadratic squeezing plate in the radial direction  $r$  with an even distribution, similar to the case where the plate is circular.

The derivation is done in a similar manner to [20], where the total squeeze force is obtained by integrating the pressure drops due to the *viscous* and the *rheological* effects. The empirical relation between the yield stress and the compressing pressure, which is also mentioned in [22], will be ignored in the mathematical model. The reasons are: that this relation could not be described physically and the parameter could only be fitted to the experimental results.

**3.2.1. Flow due to viscous effect.** As it is done in [20, equation (1)], the volumetric flow rate  $q_r(r)$  caused by the pressure difference in radial direction is

$$q_r(r) = -\frac{w(r)h^3}{12\eta} \left( \frac{\partial p_\eta}{\partial r} \right) = -\frac{\pi r h^3}{6\eta} \left( \frac{\partial p_\eta}{\partial r} \right), \quad (3)$$

where  $w$  the channel width,  $\eta$  the viscosity of the MR fluid,  $h$  the distance between the two squeezing surfaces. This distance is defined to be:

$$h = h_0 + z_q, \quad (4)$$

where  $h_0$  the initial gap of the squeezing surfaces and  $z_q$  as the displacement of the top plate in figure 8. The flow rate due to changes of gap  $h$  between two plates is

$$q_z = -A\dot{z}_q = -\pi r^2 \dot{z}_q, \quad (5)$$

with  $A$  as the area of the squeezing surface and  $\dot{z}$  as the velocity of the top plate. Due to the continuity equation, the volumetric

flow rate in radial direction should be equal to the one in vertical direction  $q_r(r) = q_z$ . Combining both equations (3) and (5), the viscous pressure drop can be obtained:

$$\frac{\partial p_\eta}{\partial r} = \frac{6\eta r}{h^3} \dot{z}_q \quad (6)$$

$$p_\eta(r) = \int \frac{6\eta r}{h^3} \dot{z}_q dr = \frac{3\eta r^2}{h^3} \dot{z}_q + C \quad (7)$$

with boundary condition, that  $p_\eta(r=0) = 0$ , then the integration constant  $C = 0$ . Therefore:

$$p_\eta(r) = \frac{3\eta r^2}{h^3} \dot{z}_q. \quad (8)$$

**3.2.2. Flow due to MR effect.** As it is done in [20, equation (5)], the pressure drop due to the existence of the applied field is:

$$\frac{\partial p_{\tau_0}}{\partial r} = \frac{2\tau_0}{h} \text{sgn}(\dot{z}_q) \quad (9)$$

$$p_{\tau_0}(r) = \frac{2\tau_0 r}{h} \text{sgn}(\dot{z}_q). \quad (10)$$

**3.2.3. Total squeeze force.** The total squeeze force can be calculated by integrating the pressures  $p = p_\eta + p_{\tau_0}$  in equations (8) and (10) over the area:

$$F_d = \int p(r) dA. \quad (11)$$

It is to be noted, that there will be some error in the calculation from the integration of the area, since some surface area on the four corners of the quadratic squeeze plate in figure 8 are not covered. In order to minimize the error, the integration boundary is set to be the average radius length

$$r_m = \frac{1}{2}(l_{s,\text{short}} + l_{s,\text{long}}) = l_s \frac{(\sqrt{2} + 1)}{4} \quad (12)$$

between the shortest and the longest distance from the surface center to the surface edges, which are  $l_{s,\text{short}} = \frac{l_s}{2}$  and  $l_{s,\text{long}} = \frac{l_s\sqrt{2}}{2}$  respectively. By using the average radius  $r_m$  as the integration boundary, equation (11) becomes:

$$F_d = \int_0^{r_m} (p_\eta(r) + p_{\tau_0}(r)) \cdot 2\pi r dr \quad (13)$$

$$F_d \stackrel{(8),(10)}{=} \int_0^{r_m} \left( \frac{6\pi\eta r^3}{h^3} \dot{z}_q + \frac{4\pi\tau_0 r^2}{h} \text{sgn}(\dot{z}_q) \right) dr \quad (14)$$

$$F_d = \frac{3\pi\eta r_m^4}{2h^3} \dot{z}_q + \frac{4\pi r_m^3 \tau_0}{3h} \text{sgn}(\dot{z}_q). \quad (15)$$

The derived total squeeze force in equation (15) corresponds to the equation of the squeeze operating mode listed in [3]. The result from this mathematical model in equation (15) should be enough to give a theoretical estimation of the force generated by the MR damper, when it is operated in squeeze mode using quadratic squeezing surface.

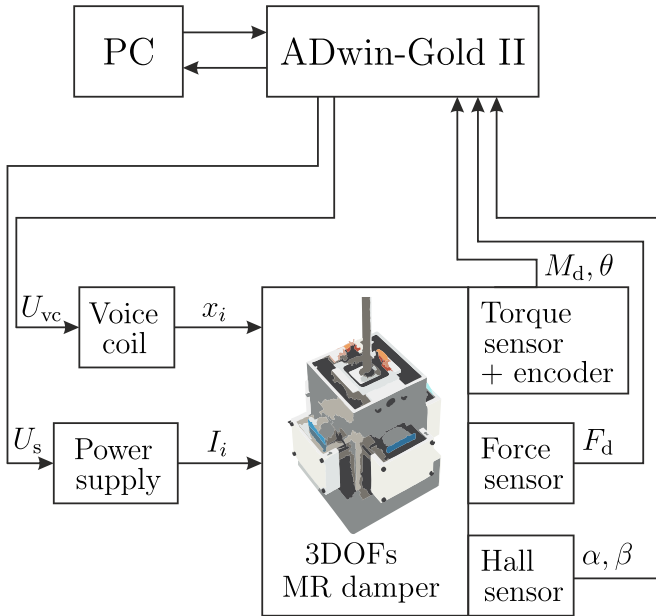


**Figure 9.** Signal flow diagram from the experimental setup used to investigate the performance of the proposed 3DOF-MR-damper.

#### 4. Experimental results and discussion

In this section, the experimental results will be presented, whereby the damper's behavior can be identified. The investigation will be divided into two aspects. The first one concerns the investigation to analyze the damping in each DOF. The second one involves the analysis of the possibility of varying the damping directions. Based on those investigations, the damper characteristics will be studied and discussed.

In automating the experiment routines and recording all the measurement data, the voice coil, the power supply, and the sensors are connected to a fast computer-controlled measurement data acquisition, ADwin-Gold II. The data acquisition board has 16 bit resolutions analog inputs and outputs and can sample the data up to a sampling rate of 100 MHz. Since all the measurements are done in a low-velocity range, the sampling rate is set to be 1 kHz. The ADwin-Gold II is connected to a computer, in which all the measured data will be saved. Figure 9 shows the signal flow diagram from this work's constructed experimental setup.

##### 4.1. Calibration of Hall sensor

As explained in section 2.2, the integrated Hall sensor measures the angular displacement  $(\alpha, \beta)$  of the rod on each axis. The measured angular displacement needs to be translated into the displacement of the damper's plunger on the  $x$ - and  $y$ -axis. This is done for two reasons:

- (a) First, the derived formula for squeeze mode results in a relation between the resulted force  $F_d$  and the distance  $h$  between the damper's plunger and the housing wall.

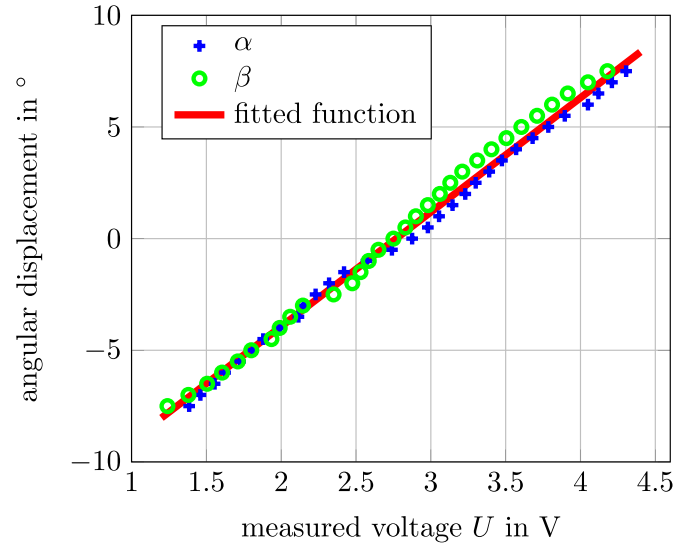


**Figure 10.** Calibration results for the Hall sensor in each axis.

- (b) Second, by displaying the force over the displacement, it is easier to imagine how close the plunger is away from the housing wall.

Figure 10 displays the calibration results for the Hall sensor on each axis. As it can be seen in this figure, the angular displacement has a linear relation to the measured sensor voltage. The damper's plunger will touch the wall after moving for 11 mm, which corresponds to the angular displacement of  $\pm 5.5^\circ$ . Therefore, the displacement of the damper's plunger on each axis is

$$x = \frac{11}{5.5}\alpha \quad \text{with} \quad \alpha = 5.12(U_x - 2.768) \quad (16)$$

$$y = \frac{11}{5.5}\beta \quad \text{with} \quad \beta = 5.12(U_y - 2.768). \quad (17)$$

The obtained displacement values will then be used to investigate the performance of the proposed 3DOF MR damper.

##### 4.2. Single DOF investigation

The three operating DOF axes of the proposed damper are the three rotating axes  $(\alpha, \beta, \theta)$ . In this part, the resulted damping force is investigated independently for each DOF.

**4.2.1. Damping in the rotational directions  $\alpha$  and  $\beta$ .** Since the damper including the four electromagnets is symmetrically constructed, the damping behavior in these axes will be identical, the results will be presented only for one of those investigated axes. Figure 11 shows the working principle diagram of the experimental setup configuration used for this investigation. As it is shown in the figure, the damper's rod is connected to the voice-coil actuator LA30-43-000A, from BEI Kimco. This actuator is guided by air bearings, which allow a smooth movement of the actuator. Since the connecting



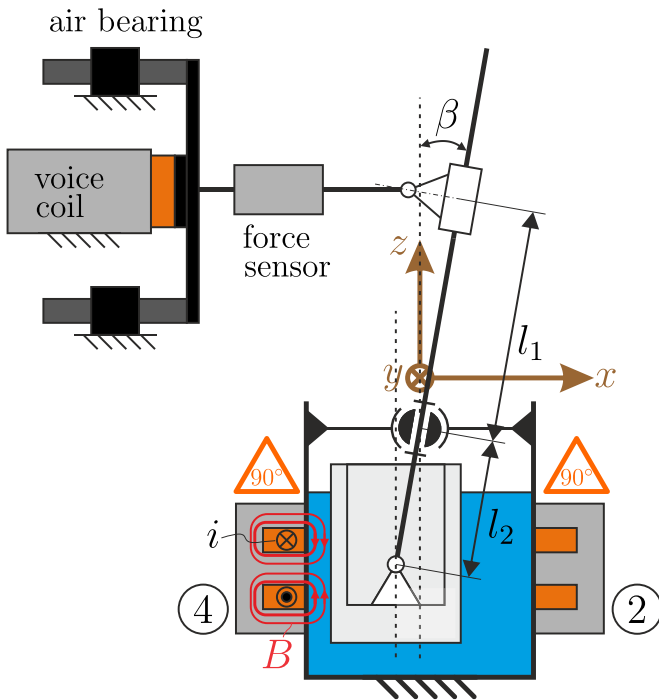


**Figure 11.** Sketch of the working principle for damping investigation in  $\alpha$  and  $\beta$ -direction.

rod is mounted to the gimbal of the damper, the translation movement of the actuator results in a rotation of the connecting rod, with the gimbal as its rotation point. Between the rod and the voice coil, a force sensor KAP-S from A.S.T. GmbH with a maximum measured force of 200 N is installed. The force sensor itself is connected via a ball joint that allows the joint to slide along the rod when the rod is rotating. When the actuator pushes the connecting rod in the positive  $x$  direction, the plunger in the fluid chamber is moved in the opposite direction. The movement of the plunger will squeeze the fluid that is located between the plunger and the wall in front of the plunger. By activating the electromagnet at the respective side of the damper, the state of the squeezed fluid between the plunger and the wall will be varied, and therefore the generated force will be increased. This generated force is then measured by the force sensor on the other side of the rod. As it can be seen in figure 11, the gimbal divides the rod into two leverages with different lengths. By using the length ratio  $l_1 : l_2 = 152 : 80$ , the actual force

$$F_d = \frac{l_1}{l_2} F_m \quad (18)$$

is obtained by scaling the measured force by the leverage's length ratio. As it is mentioned before, the measured angular displacement is then translated into displacement using equations (16) and (17). In this way, the damping can be analyzed about the  $x$  and  $y$ -axis.

For the first investigation, the plunger will be moved in one direction with a constant velocity of  $0.0048 \text{ m s}^{-1}$  and only one electromagnet will be activated. The activated electromagnet is the one at the damper side where the fluid is

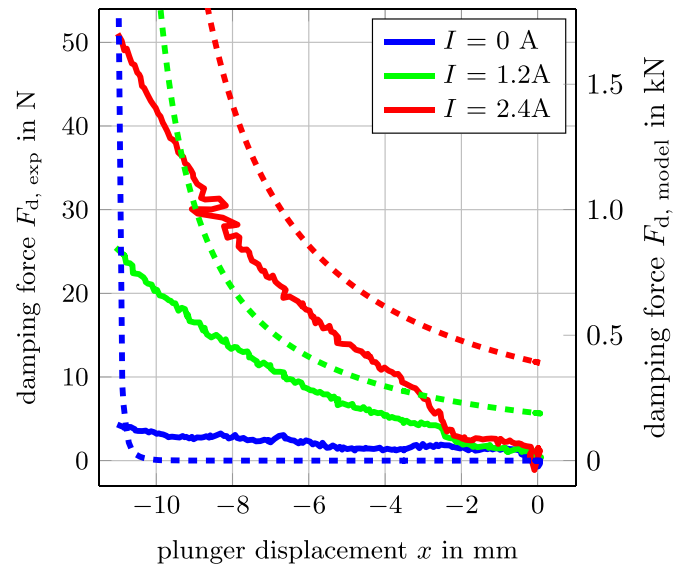


**Figure 12.** Measured damping force  $F_d$  for the damper when one electromagnet at its squeezed side is excited (continuous lines) and a calculated damping force for the conventional squeeze operation mode (dashed lines) according to equation (15).

squeezed. A really small velocity is intentionally chosen so that the increment of the damping force due to the rheological effect for increasing magnetic field can be better observed. In order to give a better orientation, the electromagnets will be enumerated as shown in figure 2. In this example, the plunger is being pushed in the positive  $x$ -direction. This made the plunger move in the negative  $x$ -direction. The fluid in the left side of the plunger is squeezed. The electromagnet No. 4 is the one to be activated to alter the state of the squeezed MR-fluid. In this way, the damping force can be varied. Figure 12 presented the experimental result of this investigation.

Since it has been informed that the plunger at its starting position has a distance of 11 mm to the wall, the measured angular displacement is presented as the displacement in the  $x$ -axis to give a better perspective on how far the plunger is to the wall. The displacement of 11 mm is the point when the plunger touched the wall of the fluid chamber. As it can be investigated from the results depicted using the straight lines, the generated force is increased as the applied current at the electromagnet is increased. Additionally to that, the force is also increased when the gap distance between the damper's plunger and the wall is getting smaller. This behavior fits the behavior of the squeeze operating mode. In this figure, calculated squeeze forces  $F_d$  from equation (15) are also presented using the dashed lines. The constant magnetic field for the conventional squeeze case are  $B = [0.0, 0.2, 0.4] \text{ T}$  for the input current value of  $I = [0.0, 1.2, 2.4] \text{ A}$  respectively. These values are obtained from the magnetic field in the FEM analysis in figure 5, approximated by the value in the middle of the damper's plunger and the chamber's wall ( $\Delta x = 5 \text{ mm}$ , as labeled in the figures). As it can be seen in the results that by using the same size of a squeezing surface, theoretically, the conventional squeeze operating mode would generate a much higher damping force, which is approximated

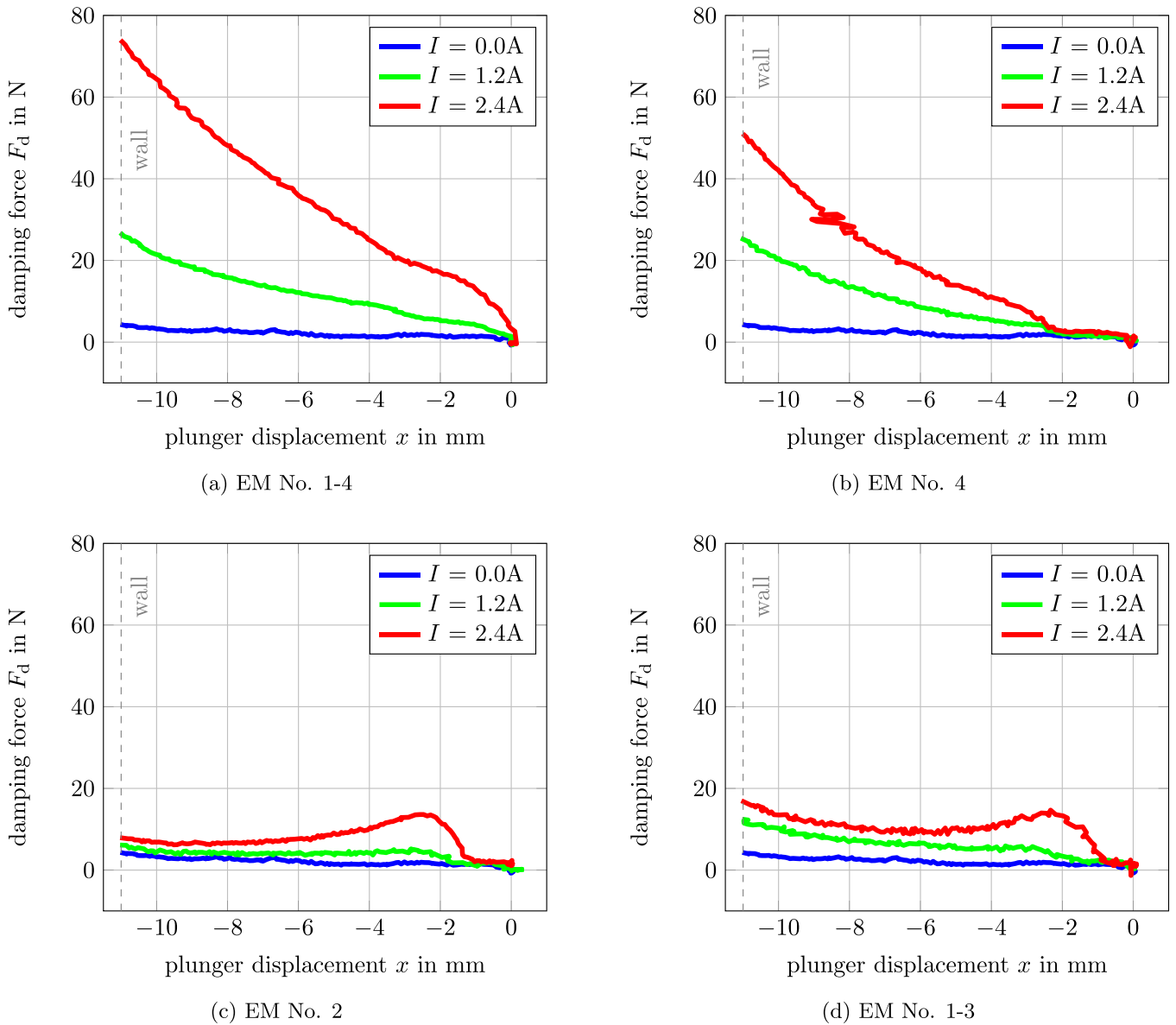


**Figure 13.** Measurement results for the investigation of the damping force along the  $x$ -axis, where the active electromagnets are (a) all electromagnets, (b) electromagnet No. 4 only, (c) electromagnets No. 2 only, and (d) electromagnets No. 1–3.

to be about  $30\text{--}40\times$  stronger in comparison to the proposed mixed-squeeze-pinch mode. Based on this evidence, it can be concluded, that the conventional squeeze operating mode in figure 6(a) with a pillar structure of the particle chain generates more resistance in comparison to the mixed squeeze-pinch mode in figure 6(b) with an arc-like chain particle structure. One reason for this may be that the arc-like particle contains more serial arranged particles compared to the pillar structure, where shorter parallel chains dominate.

The damping in this direction is not only influenced by the applied current at the electromagnet corresponding to the damping direction, No. 4, but also influenced by the other electromagnets in the fluid chamber. Since there exists only one fluid chamber in the damper, the state change of the fluid at one location could affect the flow of the fluid in the whole chamber. In investigating this aspect, the plunger is being pushed

along one movement axis (in this example, the plunger is being pushed in negative  $x$ -direction), meanwhile the activation of the electromagnets will then be varied for the same movement of the plunger. The variation is conducted for both the magnitude of the applied magnetic field, which is varied by changing the current and the number of the active electromagnets. The measurement results for this investigation are displayed in figures 13(a)–(d).

Figure 13(a) shows the measurement results for the condition when the plunger is moved against one side of the wall and all electromagnets are activated. This means that the state of the fluid is changed on all of the sides of the damper. It can be seen in the results, that for the same displacement of the plunger, the bigger the applied current is, the bigger the generated force from the damper. This verifies that the magnitude of the current is proportional to the magnitude of the created

magnetic field which results in the increment of the damping force. However, the results deliver only the resultant damping force by all activated electromagnets and do not present the share of the generated damping force from each activated electromagnet. Therefore, the same measurement is repeated for different activation patterns of the electromagnets.

Figures 13(b) and (c) present the measurement results for the condition when the plunger is moved against one side of the wall and only one electromagnet is activated. The activated electromagnet in figures 13(b) and (c) is No. 4 and No. 2, respectively. As it can be seen in figure 13(b), as the current at the electromagnet No. 4 is increased, the generated damping force  $F_d$  is also increased. This behavior is similar to the one presented in figure 13(a), yet the magnitude of the force is smaller. This is due to the reason that fewer electromagnets are activated in this measurement. This evidence also verifies that the activation of the other electromagnets has an influence on the resultant force, even though the solidified MR fluid in the other region is not the one squeezed by the damper's plunger. Contrary to this is the condition when the electromagnet No. 2 is activated (see figure 13(c)). As it can be seen through the results, there are almost no changes in the force–displacement characteristic lines, even though the current is increased. It is to be noted, that there exists an increment of the force due to the increment of the applied current only in the beginning (at about  $-1$  mm). This effect is suspected to be caused by the fluid that is affected by the magnetic field from electromagnet No. 2. As soon as the plunger moved away, the effect of the magnetic field on the MR fluid is reduced significantly (see the finite element results in figure 5). On the other side of the plunger, the fluid is squeezed yet the state of the fluid is unchanged since there is no magnetic field applied. Therefore, the force–displacement characteristic line is similar, starting from a displacement of about  $-4$  mm until the plunger reached the wall at  $-11$  m.

The next experiment is for the case where all electromagnets (No. 1–3) are activated except the one at the squeezed side (No. 4). Even though it is small, the other three electromagnets have however influences on the total generated damping force. This can be seen in the measurement result in figure 13(d). There exists an increment of force as the current is increased. However, the increment is much smaller in comparison to the one in figure 13(b). This is supporting evidence for the analysis of the measurement results in figure 13(b).

From the measurement results presented in figures 13(a)–(d), it can be concluded that the increment of the force due to the rheological effect is dependent on the applied current. The main contribution of the damping forces is the result of activating the electromagnet at the squeezed side of the damper. In addition to that, the activation of the other electromagnets has a contribution to the total generated force. This should be deeper investigated when the movement of the plunger is more complex.

In giving a direct insight into how the dissipation of the device increases by increasing velocity and magnetic field, a harmonic excitation is given to the plunger. The voice coil is controlled to give the plunger a sinusoidal movement with

varying frequencies. The excitation function for this investigation is described as follows:

$$x(t) = X_{\text{off}} + X \sin\left(2\pi ft - \frac{\pi}{2}\right), \quad (19)$$

with  $f$  as the excitation frequency,  $X$  as the amplitude, and  $X_{\text{off}}$  as the offset of the excitation signal. By adding the offset of its amplitude ( $X_{\text{off}} = X$ ) and a phase shifting of  $\frac{\pi}{2}$ , the initial displacement  $x_0$  and initial velocity  $\dot{x}_0$  can be started from 0. As the frequency varied, the applied current is also varied. For this investigation, the chosen excitation frequencies are  $f = [0.053, 0.105, 0.210]$  Hz. The same input current values of  $I = [0.0, 1.2, 2.4]$  A are chosen to give a comparable results. The results are plotted in figure 14 as force–velocity graphs.

The four force–velocity plots in figure 14 show the hysteretic behavior of the proposed MR damper. The small arrow indicates the direction of the hysteresis loop. The hysteresis loop is represented by the enclosed area in the force–velocity plot. Figures 14(a) and (c) show the resulting forces for varying excitation frequencies when the applied current  $I$  of 1.2 A and 2.4 A respectively are held constant. As can be seen in both figures, the increasing frequency, and therefore, the increasing velocity results in an expansion of the enclosed area of the hysteresis in the horizontal direction (along the velocity axis). Figures 14(b) and (d) show the resulting forces for varying the applied current when the excitation frequencies  $f$  of 0.105 Hz and 0.210 Hz respectively are held constant. In comparison to the case where the excitation frequency is varied, the increasing applied current, and therefore, the increasing magnetic field results in an expansion of the enclosed area of the hysteresis in the vertical direction (along the force axis). It can be observed, that the increment of both excitation frequency and the applied current results in an expansion of the enclosed area of the hysteresis loop, which corresponds to the dissipation energy resulting from the MR damper.

The irregular form of the hysteresis loop is caused by the nonlinear behavior of the proposed mixed squeeze-pinch operating mode. Moreover, the displacement is excited only in one direction from the middle point of the damper, which results in asymmetric hysteresis plots. The investigation up to this point is however enough to verify the variation of the dissipation energy resulting from the proposed 3DOF MR damper. Further investigation in regards to the modeling of this hysteretic behavior is suggested to be done as future work.

**4.2.2. Damping in rotational direction  $\theta$ .** The next investigation is to investigate the variation of the torque based on the applied current. This will be the third DOF, the direction about the  $z$ -axis. The sketch of the working principle for this investigation is presented in figure 15. As it is shown in this figure, the rod is not connected to the voice-coil actuator anymore. Instead, it is connected to leverage, whereby the connecting rod and therefore the plunger is rotated about the  $z$ -axis. Between the leverage and the rod, a torque sensor Typ 4503A from Kistler Lorch GmbH is installed. This torque

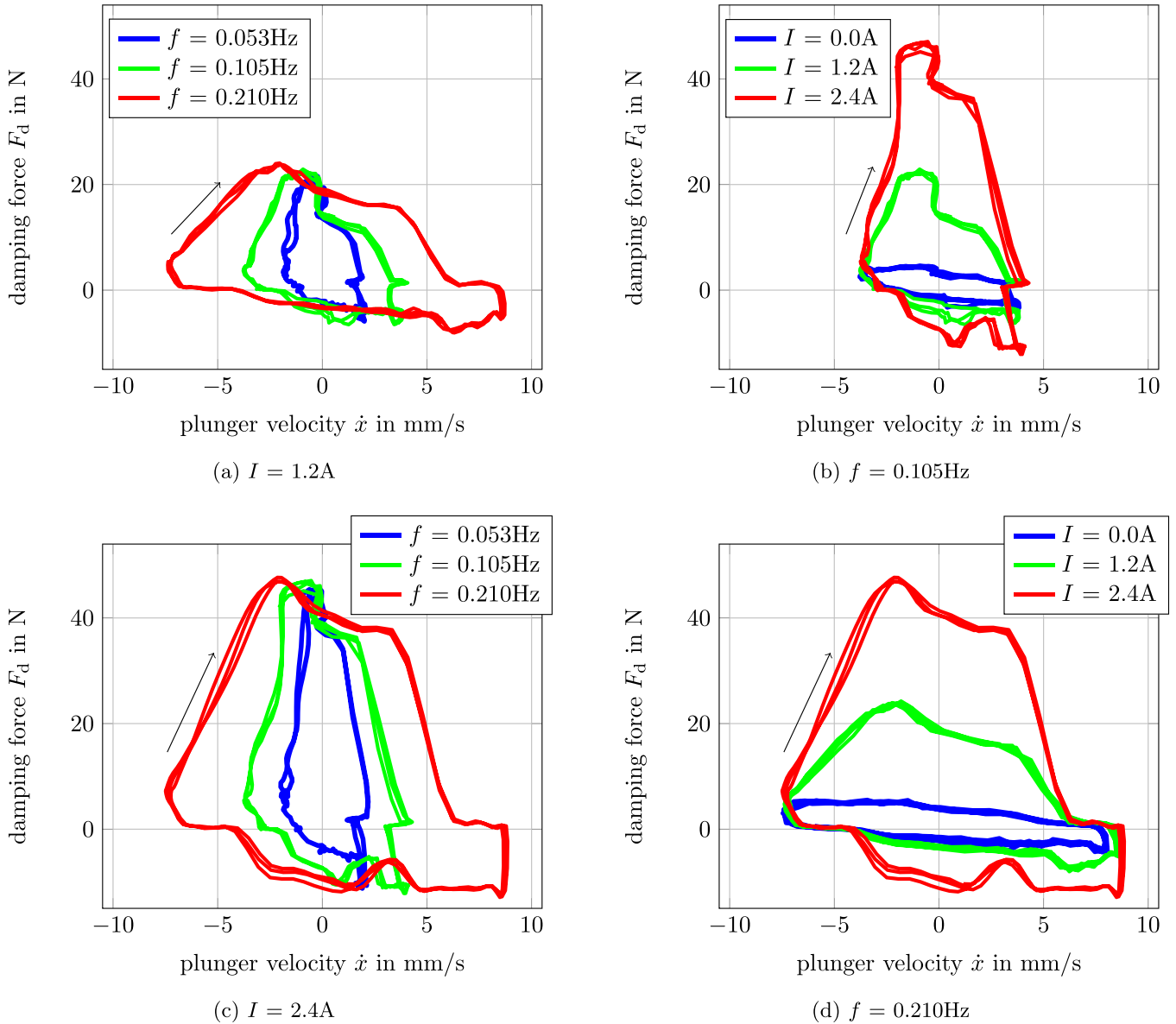


**Figure 14.** Damping force over plunger velocity with varying excitation frequencies for a constant applied current of (a) 1.2 A and (c) 2.4 A; and varying applied currents for a constant excitation frequency of (b) 0.105 Hz and (d) 0.210 Hz.

sensor is mounted to the ground via frame support. The mounting has been constructed so that the torque sensor is concentric to the rod when the rod is exactly perpendicular to the ground ( $\alpha = \beta = 0^\circ$ ). This torque sensor has an integrated encoder, which can be used directly to measure the rotation angle  $\theta$  and connected to a rod via a coupling, that eliminates unwanted force on the torque sensor itself.

For this experiment, the plunger is rotated at an angular velocity of  $0.628\text{ rad s}^{-1}$ . During the rotation, a current and therefore a magnetic field is applied in the fluid chamber (figure 16). The figure shows that the measured torque is increased as the current is increased. This is once again caused by the solidified MR fluid due to the current. The bigger the current is, the harder it is for the plunger to rotate. However, using this box damper design, the torque is not evenly distributed about the angle of rotation  $\theta$ . As it can be seen in

the results, the torque reaches its maximum when the plunger is rotated by  $45^\circ$  and multiples ( $\theta = \frac{\pi}{4} + n\frac{\pi}{2}$  for  $\theta \in [0, 2\pi]$  with  $n = 0, \dots, 3$ ). The minimum torque is reached when the plunger is rotated by  $90^\circ$  and multiples. This is the position when the plunger wall is parallel to the chamber's wall.

#### 4.3. Independent adjustment of damping

For the last investigation in this work, the generated damping direction is investigated. The purpose of this investigation is to seek the possibility of having damping be increased only in one specified direction. Figure 17 depicts the sketch of the working principle of the experimental setup used for this purpose. The main difference between this setup in comparison to the previous two investigations is the additional spring. This spring is necessary to get an oscillatory system.

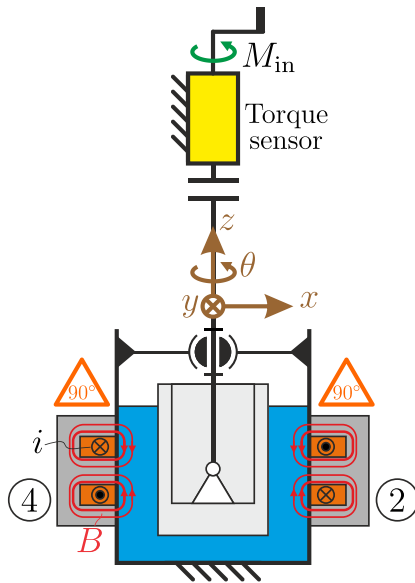


Figure 15. Sketch of working principle for damping investigation about the z-axis.

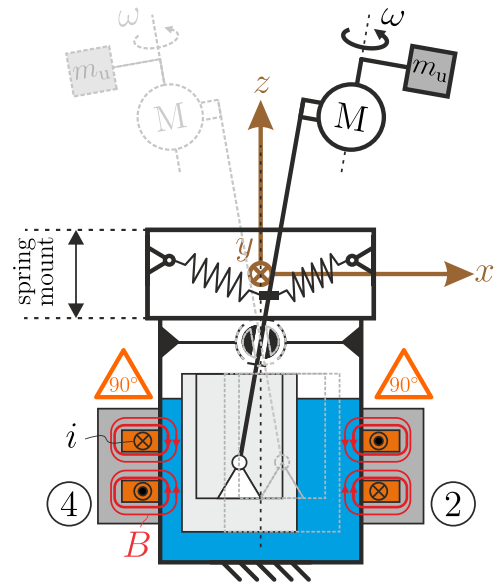


Figure 17. Sketch of working principle for damping investigation in different directions.

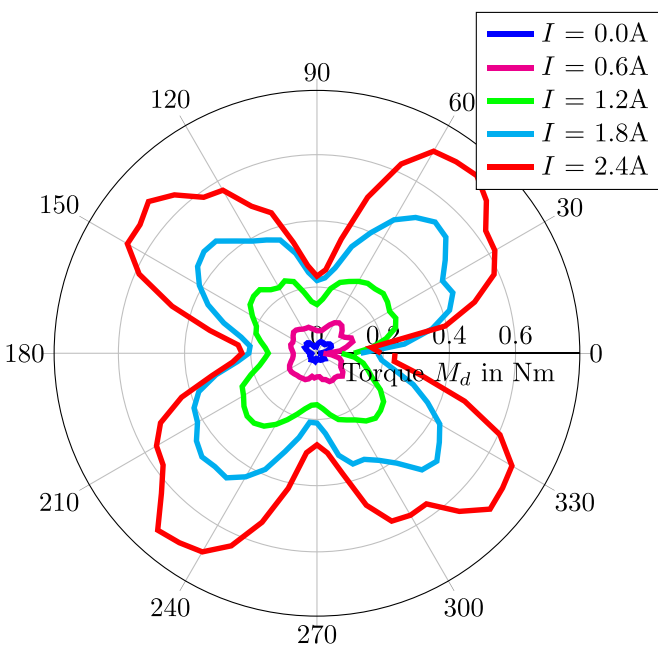


Figure 16. Measurement results of the generated damping torque  $M_d$  at about the z-axis.

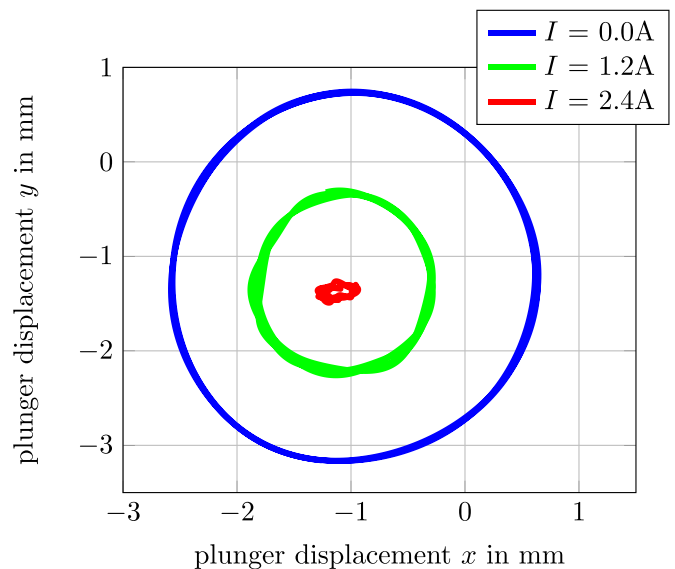


Figure 18. Measurement of the damper's plunger displacement when the imbalance mass is rotated to excite the plunger and all electromagnets are activated.

The vibration itself is generated by a rotation of an imbalance mass  $m_u$ , attached to the free end of the connecting rod. This mass is mounted to a motor with a certain length of leverage and rotated by a DC motor  $M$ . When the mass  $m_u$  is rotated, the connecting rod and therefore the damper plunger inside the fluid chamber will be rotated as well. Due to the existence of the springs, vibrations are created.

The measurement results can be seen in figure 18. The vibration due to the imbalance acts in two different directions. This can be seen from the measurement of the angular displacement in each  $x$ - and  $y$ -axis, represented by the blue

lines. This is the condition when none of the electromagnets are activated. By activating all of the electromagnets, the vibration of the plunger is dampened in all directions, as seen in figure 18. The stronger the applied field (the higher the current), therefore the stronger the damping. This can be seen by the reduction of the circle area in the results. A smaller circle means that the damper plunger moves less in both  $x$  and  $y$ -axes. It can also be seen that the center of rotation is not at the point  $(0,0)$ . This is caused by the additional mass from the motor and the imbalance, which is not mounted in the system's center of inertia.

In another case, when the damping is only required in one specific direction, the activation of the electromagnet only

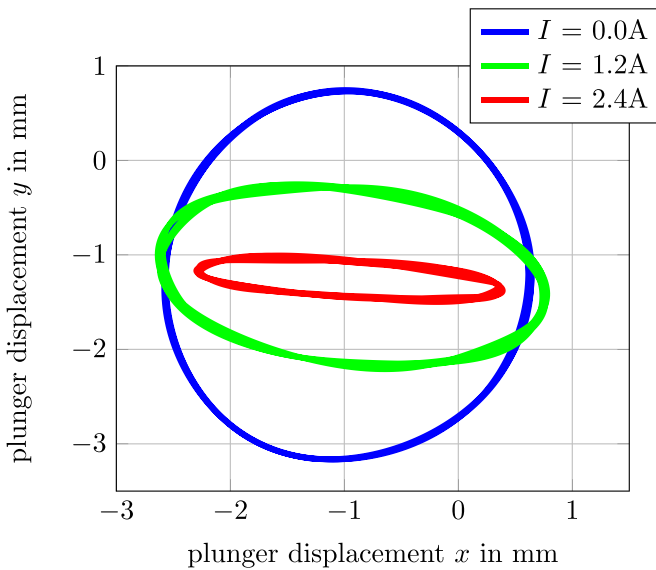


**Figure 19.** Measurement of the damper's plunger displacement when the imbalance mass is rotated to excite the plunger and the electromagnets are activated in pair.

needs to be conducted for the electromagnet that is installed in the respective axis. As it can be seen in figure 19, the vibration amplitude is only reduced along the  $y$ -axis, meanwhile, the vibration amplitude along the  $x$ -axis remains unchanged. This is achieved by activating the two electromagnets installed along the  $y$ -axis, meanwhile leaving the other two electromagnets along the  $x$ -axis unactivated. The results show that the circle has become an oval. It means that the movement in the  $y$ -axis is smaller than the movement in the  $x$ -axis. It also can be seen that the oval will be smaller as the current is increased. This verifies the ability of the damper to only generate damping in one specified direction.

## 5. Conclusion

In summary, a new design of a 3DOF MR damper is proposed and constructed. The three DOFs are the three rotational displacements ( $\alpha$ ,  $\beta$  and  $\theta$ ). Experiments and investigations are made, where the damper's behavior is analyzed for a damper movement not only in one single DOF but also in several DOFs.

It can be concluded that the concept works as expected, where the damping can be generated in all three DOFs, both individually or together. In addition to that, the damping can be generated to be dominant in one specific direction. In comparison to the conventional squeeze mode, the resulted force is predicted to be smaller. This is due to the reason, that the

particle chain has a shape of an arc and therefore a weaker fluid resistance can be achieved. It is also to be noted, that by connecting the damper with a ball joint, as done in figure 11, the damping for the rotational displacement ( $\alpha$  and  $\beta$ ) can be converted into damping for translational displacements in the  $x$ - and  $y$ -axes.

Based on the results presented in this work, the proposed concept can be used not only as a damper for the 3DOF vibration system but also as an actuator, for example as a haptic device. As a multi degrees-of-freedom (MDOF) MR damper, its potential has been shown by the results in figures 18 and 19, where the damping can be generated in both single and multiple directions. As a haptic device, this effect can be used to allow a movement in one direction, meanwhile blocking the movement in the other unwanted directions. Additionally, this configuration offers a compact size damper, which potentially can result in reducing the required installed size in comparison to the conventional method, if a proper design is conducted. As an option, this design offers a simple scaling possibility for the operating region. This can be done by changing the length of the connecting rod.

For future works, the behavior of the mixed squeeze-pinch mode used in this work needs to be further investigated. Furthermore, an analytical model for the mixed squeeze-pinch mode should be proposed, whereas the model can be used to do a parametric design of such damper utilizing this mixed mode. Additionally to that, the hysteresis behavior and influence should be investigated to allow a proper control design for this 3DOF MR damper. There is also a possibility to improve the mechanical design by using a circular housing and plunger instead of the quadratic one. In this way, the plunger will have an equal displacement range in all directions, and therefore a combined damping effect can be better investigated. However, the performance of the damper with circular housing and plunger should be characterized to show the comparison.

## Data availability statement

The data generated and/or analyzed during the current study are not publicly available for legal/ethical reasons but are available from the corresponding author on reasonable request.

## Acknowledgment

The authors would like to express their gratitude towards the German Research Foundation, *Deutsche Forschungsgemeinschaft* (DFG) for the financial support within the priority program SPP 1897, 'Calm, Smooth, and Smart'.

## Appendix A. Parameters

**Table A1.** Geometry parameters of the proposed 3DOF compact MR damper.

Physical property	Value	Unit
Housing		
• length	78	mm
• width	78	mm
• height	100	mm
Plunger		
• length	56	mm
• width	56	mm
• height	84.5	mm
Initial gap to each wall $h_0$	11	mm
Electromagnet		
• number of winding $N_c$	315	
• wire diameter $d_{Cu}$	0.63	mm
• max. current $I$	2.4	A

## ORCID iD

Aditya Suryadi Tan  <https://orcid.org/0000-0001-5545-4702>

## References

- [1] Wereley N 2014 *Magnetorheology : Advances and Applications* (United Kingdom: The Royal Society of Chemistry)
- [2] Elahinia M, Ciocanel C, Nguyen T M and Wang S 2013 MR- and ER-based semiactive engine mounts: a review *Smart Mater. Res.* **2013** 1–21
- [3] Zhu X, Jing X and Cheng Li 2012 Magnetorheological fluid dampers: a review on structure design and analysis *J. Intell. Mater. Syst. Struct.* **23** 839–73
- [4] Wang D H and Liao W H 2011 Magnetorheological fluid dampers: a review of parametric modelling *Smart Mater. Struct.* **20** 023001
- [5] Nguyen T, Elahinia M, Walter W O and Fontaine P 2006 A 6-DOF vibration isolation system for hydraulic hybrid vehicles *Proc. SPIE* **6169** 102–12
- [6] Weber F and Distl H 2015 Amplitude and frequency and Ruskky bridge by magnetorheological dampers *Struct. Control Health Monit.* **22** 237–54
- [7] Spelta C, Previdi F, Savaresi S M, Fraternali G and Gaudiano N 2009 Control of magnetorheological dampers for vibration reduction in a washing machine *Mechatronics* **19** 410–21
- [8] Jong-Seok O, Woo Sohn J and Choi S-B 2022 Applications of magnetorheological fluid actuator to multi-DOF systems: state-of-the-art from 2015 to 2021 *Actuators* **11** 44
- [9] Xuan Phu D and Choi S-B 2015 Vibration control of a ship engine system using high-load magnetorheological mounts associated with a new indirect fuzzy sliding mode controller *Smart Mater. Struct.* **24** 1–20
- [10] Jong-Seok O and Choi S-B 2017 State of the art of medical devices featuring smart electro-rheological and magneto-rheological fluids *J. King Saud Univ. Sci.* **29** 390–400 SI: smart materials and applications of new materials
- [11] Ahmadvkhanlou F, Washington G N and Bechtel S E 2009 Modeling and control of single and two degree of freedom magnetorheological fluid-based haptic systems for telerobotic surgery *J. Intell. Mater. Syst. Struct.* **20** 1171–86
- [12] Nguyen H Q, Thang L, Nguyen D N, Le T D, Lang T V and Ngo T 2020 Development of 3-DOF force feedback system using spherical arm mechanism and MR brakes *Int. J. Mech. Eng. Robot. Res.* **9** 170–6
- [13] Tri Diep B, Diep Nguyen N, Tran T T and Hung Nguyen Q 2020 Design and experimental validation of a 3-DOF force feedback system featuring spherical manipulator and magnetorheological actuators *Actuators* **9** 2020
- [14] Song B-K, Jong-Seok O and Choi S-B 2014 Design of a new 4-DOF haptic master featuring magnetorheological fluid *Adv. in Mech. Eng.* **6** 843498
- [15] Jong-Seok O, Choi S-H and Choi S-B 2014 Design of a 4-DOF MR haptic master for application to robot surgery: virtual environment work *Smart Mater. Struct.* **23** 095032
- [16] Arus MR Tech Pvt Ltd, 3/27, M.H Road, Chennai-600 011 2021 *AMT-SMARTEC*
- [17] Goncalves F D and Carlson J D 2009 An alternate operation mode for MR fluids—magnetic gradient pinch *J. Phys.: Conf. Ser.* **149** 012050
- [18] Lee T-H, Kang B-H and Choi S-B 2019 A quasi-static model for the pinch mode analysis of a magnetorheological fluid flow with an experimental validation *Mech. Syst. Signal Process.* **134** 106308
- [19] Joseph H S and Aksel N 2010 *Fluid Mechanics* (Berlin: Springer)
- [20] Farjoud A, Cavey R, Ahmadian M and Craft M 2009 Magneto-rheological fluid behavior in squeeze mode *Smart Mater. Struct.* **18** 095001
- [21] de Vicente J, Antonio Ruiz-López Je, Andablo-Reyes Een, Pablo Segovia-Gutiérrez J and Hidalgo-Alvarez R 2011 Squeeze flow magnetorheology *J. Rheol.* **55** 753–79
- [22] Tao R 2001 Super-strong magnetorheological fluids *J. Phys.: Condens. Matter* **13** R979–99